1st year Transfer report

Dustin McGivern

June 14th 2002

Abstract

This report gives an outline of the run 2 upgrades to the Tevatron and CDF and a description of preliminary investigations into the measurement of diboson production with run 2 data including comparisons of next to leading order diboson event generators.

1 Tevatron run 2 and the CDF upgrade

1.1 Tevatron run 2

For the current run, run 2a, the Tevatron has undergone many improvements. The luminosity is being increased to $5 \times 10^{31} cm^{-2}s^{-1}$ from $1 \times 10^{31} cm^{-2}s^{-1}$, in run 2b this will be increased further to $2 \times 10^{32} cm^{-2}s^{-1}$. This larger luminosity is driven by an increase in the number of protons and anitprotons per store delivered by the new main injector which has replaced the main ring of run 1. The main injector complex also contains a new recycling facility that allows unused antiprotons to be saved at the end of the store and used for the next one. The number of bunches has increased from 6×6 in run 1 to 36×36 in run 2a and eventually 140×121 in run 2b. The large increase in the number of bunches in run 2b is needed to decrease the number of interactions per bunch crossing from 6 to 2 or 3. Consequently the bunch spacing of 396ns in run 2a will be reduced to 132ns in run 2b. Finally the centre of mass of the collider has also been increased to $\sqrt{s} = 1.96$TeV.

The highest luminosity that has so far achieved is $2 \times 10^{31} cm^{-2}s^{-1}$, this will be increased as improvements are introduced during the June shutdown and the longer September shutdown. The final target of $5 \times 10^{31} cm^{-2}s^{-1}$ will be reached when the recycling facility has finished commissioning and goes into full operation. Between mid January 2002 and June 30 2002 CDF collected an total integrated luminosity of $30pb^{-1}$.

1.2 CDF upgrade

The improvements in the Tevatron have lead to upgrades of both CDF and D0. The majority of the improvements to the detectors is driven by the increase in luminosity and new bunch structure rather than the change in centre of mass energy. The upgrades to CDF[2]essentially address three areas: improved tracking, increased kinematic coverage and improved tagging of displaced verticies.

1.2.1 Tracking

The entire tracking volume of the CDF detector has been replaced, although the general design, silicon surrounded by gas, has remained. The new silicon sub detector is separated into different sections. Layer00 is mounted on the beam pipe itself to give an accurate measurement of the track impact parameters. The inner tracker comprises of a five layer detector at small radii for secondary vertex reconstruction (SVX2) and then two additional layers at a larger radii to provide Pt resolution and b-tagging (ISL). These systems do however operate as a single sub detector. The silicon will be capable of producing stand alone tracking to $|\eta|<2.0$ with a fully pipelined output to handle the eventual 132ns bunch separation (achieved by mounting the readout chips on the silicon itself). The new gas chamber, the central outer tracker (COT) has 6 times more wires than the old run1 chamber and also has a reduced drift time of 132ns to reduce occupancy problems associated with the new and the eventual bunch structures.

1.2.2 Muon

The muon system is made up of scintillators, proportional chambers and absorbers, namely the calorimeter steel, return magnet yoke and additional steel walls. The changes to the muon detector are designed to fill the gaps of the old system and extend its reach to $|\eta|<1$.

1.2.3 Trigger and DAQ

For run 2, CDF has an entirely new three level trigger and DAQ system. The first two levels are hardware based and the third is a processor farm. Level one uses regional information from the fastest sub-detectors to make an outline of the objects in the event, such as basic jets and photon-like objects from the calorimeter information and some tracking information to identify electrons and muons. At level two, silicon information and more accurate track and muon data are added to make a more accurate sketch of the event before it is passed to Level 3 where all of the event information is collated for the first time. This can be considered the first stage of the full event reconstruction and analysis. Level 3 provides a way to sort the different classes of interactions based upon reconstruction code similar to that used offline and deciding whether the event is interesting enough to be written to permanent storage.

2 Diboson pair production

2.1 Introduction

The Standard Model makes specific preditions for the trilinear gauge boson couplings of the W,Z and γ bosons. A measurement of these couplings is a vital test of the very nature of the theory and possible point of discovery of new physics. Hence a measurement of the WW cross-section is an important test of these couplings. It is also essential that this processes is well understood since it is such a major background in the eventual measurement of $H \rightarrow WW$ and other exotic physics signals in the lepton plus missing Et channel. The decay channels focused on in this report are $WW \rightarrow e\nu e\nu$ and the more difficult $WW \rightarrow e\nu jj$ channel where the backgrounds are larger.

2.2 Theory of diboson production and anomalous couplings

In the standard model the W,Z and γ may couple to each other in a number of different ways as shown in Fig 8. The most general Lagrangian for these interactions(considering operators up to dimension 6 only) contains some 14 different coupling parameters[8]. Many of these couplings would diverge with energy and violate unitarity, hence there would have to be new physics entering to counter this

Table 1: Run 1 event yields and cross-sections for WW production

Mode	L	Data	Background	$\sigma^{diboson}_{meas}$	$\sigma^{diboson}_{theory}$
$(l = e, \mu)$	(pb^{-1})	(events)	(events)	(pb)	(pb)
$W\gamma \to l\nu, \gamma$	67	109	26.4 ± 3.6	20.7 ± 3.0	18.6
$WW \to l\nu, l\nu$	110	5	1.21 ± 0.30	$10.2^{+6.5}_{-5.3}$	9.5
$WZ \to l\nu, ll$	110	1	$0.3^{+0.8}_{-0.3}$	$3.2^{+5.0}_{-3.2}$	2.5
$Z\gamma \to ll, \gamma$	67	31	1.4 ± 0.4	5.7 ± 1.4	4.8
$ZZ \to ll, ll$	120	1	?	?	1.0

divergence. In the standard model therefore, these coupling are set to zero. This report will consider only the surviving, CP conserving couplings ${g_1}^z$, κ_γ, λ_γ, κ_z and λ_z . These are the couplings which describe the WWZ and WWγ verticies. In the standard model $\lambda_\gamma = \lambda_z = 0$ and ${g_1}^z$,κ_γ and κ_z are set to 1, or in the more usual notation $\Delta\kappa_\gamma = \kappa_\gamma - 1 = 0$ and similarly for ${g_1}^z$ and κ_z.

2.3 Diboson production at the Tevatron

These couplings are investigated at CDF by studying the production of Wγ and Zγ events and WW, WZ or ZZ pair production(Fig 8).

The pair production events can be used to set limits on all four couplings, however separating the $WW\gamma$ component from the WWZ component is not easy; it is usual to make some further simplifying assumption(eg, $\Delta\kappa_\gamma = \Delta\kappa_z$and $\lambda_\gamma = \lambda_z$). The W$\gamma$ and Zγ events are used to place limits directly on $\Delta\kappa_\gamma$ and λ_γ, this is somewhat cleaner since there is no interference from a Z vertex.

It is worth noting that WW pair production has a distinct advantage over the other types of event because the cross-section has terms proportional to the anomalous coupling $\Delta\kappa_V$ which grow like $\hat{s}/M_W^2$. In the other processes the terms in the cross-section are proportional to $\sqrt{\hat{s}}/M_W$ only.

2.4 Current measurements and run2 expectations

2.4.1 run 1

In run 1 the measurements were initially made with $67pb^{-1}$ of combined e and μ data and then updated with $100pb^{-1}$ of data[2], giving results for the cross-section and event yields as shown in table 1. The anomalous coupling limits were set (assuming $\Delta\kappa_\gamma = \Delta\kappa_Z$, $\lambda_\gamma = \lambda_Z$ and $\Delta g_1^z = 0$) at:

- $-1.8 < \Delta\kappa_\gamma < 2.0$ and $-0.7 < \lambda_\gamma < 0.6$ at the 95% CL using $W\gamma$ and $W\gamma$ events.
- Using the run 1a and 1b data no clean $WW, WZ \to l\nu jj$ events were observed and limits of -0.7$<\Delta\kappa_Z<$0.9 and -0.5$<\lambda_Z<$0.5 were placed at the 95% CL.

Although there was no direct measurement of the SM WWZ coupling in run 1, the lack of any excess of high-pt WW events in the data was shown to exclude a zero-strength WWZ coupling at $>$99%CL[2] (if the WWZ coupling was zero then the γWW-ZWW gauge cancellations predicted by the standard model would not exist and so WW production would be at the larger γWW level)

Table 3: LEP2 2001 Anomalous coupling limits. Set at the 95%CL assuming a SU(2)× U(1) relationship between the γ and Z couplings

$-0.087 < \Delta g_1^z < 0.141$
$-0.200 < \Delta\kappa_\gamma < 0.258$
$-0.062 < \lambda_\gamma < 0.147$

2.4.2 LEP2 results

The updated 2002 LEP2 results have not yet been published. The most recent LEP2 combination result is from summer 2001[1] which reports the coupling limits of table 2.

2.4.3 run 2

In run 2 the production cross-section for $p\bar{p} \rightarrow WW$ will increase to $10.1pb^{-1}$, with this additional cross-section and the higher luminosity significant improvement over run 1 is expected. Based upon the run 1 analysis, the expected limits with $2fb^{-1}$ of run2 data are ± 0.3 on $|\Delta\kappa_V|$ and ± 0.1 on $|\lambda_V|$ and so comparable with the LEP2 results of table 2.

Run 2 Wγ and Zγ event yields are expected to be ~1500 and 450 respectively, indicating significant improvement on the run1 limits set with 109 Wγ events and 31 Zγ events.

In run 1 the $WW \rightarrow l\nu l\nu$ events were primarily central and so the upgrades to the central muon system and the additional acceptance of run 2 gives much hope of an improved measurement. For $2fb^{-1}$ the standard model predicts ~100 WW dilepton pairs will be observed in run2.

Even though the $WW \rightarrow e\nu jj$ channel is far more difficult to measure due to the large backgrounds, it is hoped that through the use of advanced analysis techniques, such as neural networks, enough improvements can be made for this measurement to be made.

3 Simulation of diboson production with anomalous couplings

3.1 Introduction

In general the inclusion of anomalous couplings causes an enhancement of the WW cross-section[5], especially at large values of the transverse momentum of the W bosons. It has also been shown that O(α_S) corrections of hadronic WW production are significant in precisely this region[10][6]. It is therefore of great importance to use next to leading order(NLO) calculations when investigating WWV vertices.

There are a variety of next to leading order programs for hadron-hadron colliders in existence. This section will be concerned mainly with a comparison of two programs; Baur et al (BHO) and Campbell & Ellis (MCFM).

BHO is the program by Baur et al[5] used in the run 1 CDF analysis. It suffers from one main deficiency, namely that the lepton correlations are only partially included, ie the W decays isotropically for the virtual terms. For the purposes of a measurement of diboson production BHO also lacks a simulation all of the processes of interest (such as $WW \rightarrow e\nu jj$). MCFM[7] is a program by John Campbell et al that contains full correlations, singly-resonant contributions and all required processes. For completeness there is another program by Dixon et al[9] that contains full correlations and anomalous couplings but it will not be discussed here.

3.2 BHO

This program is a calculation by Baur et al[5] of the process $WW \rightarrow e\nu e\nu$ at next to leading order. The calculation is performed using the narrow width approximation for the leptonically decaying W bosons, it includes contributions from the square of the born(leading order) graphs, the interference of the born and one-loop virtual graphs and the square of the real emission graphs. The difficulty in making the calculation arises from the fact that the real emission graphs, in the limit that the gluon is soft or collinear, are singular. The BHO program isolates these singularities by splitting up phase space into soft, collinear and finite regions and then explicitly cancelling the infrared singularities and absorbing the others into the definition of the parton distribution functions.

3.3 MCFM

This program aims to give a unified description of processes involving final states with heavy quarks, leptons and missing energy at next-to-leading-order accuracy. This program is the only one available that is capable of simulating $WW \rightarrow e\nu jj$ at next to leading order.

As with BHO, there are three major contributions, the lowest order Born contributions, the virtual(loop) corrections and the real corrections associated with additional soft or collinear radiation. The singularities are dealt with using the general subtraction procedure of Ellis et al[4]. MCFM has an additional contribution from singly resonant diagrams that arise from the final state of four leptons that would be overlooked in a calculation with a final state of two bosons.

The program includes the following processes:

- $p\bar{p} \rightarrow W/Z, W+Z, WW, ZZ, W/Z+H, H, W+g(\rightarrow b\bar{b})$
- $p\bar{p} \rightarrow W+2jets, W/Z+1jet, Z/\gamma+b\bar{b}, Z/\gamma+2jets$

plus the leptonic/hadronic decays of the bosons included as sub-processes. Many of the NLO matrix elements are obtained by crossing the ones calculated for $e^+e^- \rightarrow 4jets$.

3.4 MCFM vs BHO

Comparisons of the two programs were made by producing 1.4million *weighted* $WW \rightarrow e\nu e\nu$ events with each program and comparing both the predicted SM cross-section (see table 5) and the cross-section as a function of the anomalous couplings (see Figs 1 and 2). Plots comparing the kinematic distributions of the final state particles are shown in Figs 5 to 7.

3.4.1 Standard Model cross-section predictions

The programs were run using the zero width approximation for the W bosons (since BHO can only run in zero width limit) using the mrs96r2 parton distribution functions, for a centre of mass energy of 2.0TeV and the QCD scale set to 100GeV.

The difference in cross sections in table 5 above is ascribed to a difference in the value of $\sin 2\theta_w$ [1] used by the two programs. The cross-section predictions of MCFM were also found to vary by $6-7\%$ for different parton distribution functions and by about $3-4\%$ when the width of the W is included.

[1]under investigation

Table 5: SM cross-section predictions of MCFM and BHO

Program	NLO SM cross-section	LO SM cross-section
MCFM	$146.7 \pm 0.2pb^{-1}$	$108.2 \pm 0.3pb^{-1}$
BHO	$127.1 \pm 0.9pb^{-1}$	$97.2 \pm 0.8pb^{-1}$

3.4.2 Anomalous coupling vs cross-section

The programs were run for a variety of values of the anomalous couplings to examine how the predicted cross-section behaves as a function of these couplings. Each coupling was examined in turn, varying its value from -3 to 3 keeping all other couplings at their SM values. The minimum in the fit to the data points represents the predicted SM cross-section, clearly showing that the cross-section is greatly enhanced by any non-SM coupling. The plots also show that any variation in $\Delta\kappa_z$ or λ_z has a much larger effect on the cross-section than the same variation in $\Delta\kappa_\gamma$ or λ_γ.

3.4.3 The kinematic distributions

Fig 5 shows the predicted transverse momentum of the W bosons and WW pair, Fig 6 shows the mass of the WW pair and Fig 7 shows the rapidity plots of the electrons and positrons. Except for the difference in cross-section there is good agreement between MCFM and BHO on the pt plots of the individual W's and the mass of the WW pair, but they do not agree on the pt distribution of the WW pair. The

Figure 1: MCFM cross-section vs anomalous coupling. From top left to bottom right: Δg_1^z , $\Delta\kappa_z$, $\Delta\kappa_\gamma$, λ_z , λ_γ

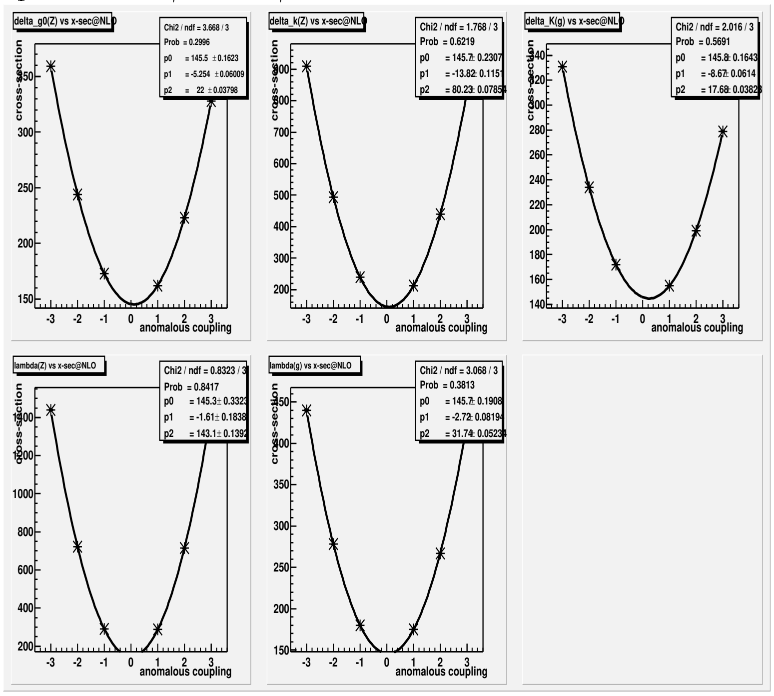

Figure 2: BHO cross-section vs anomalous coupling

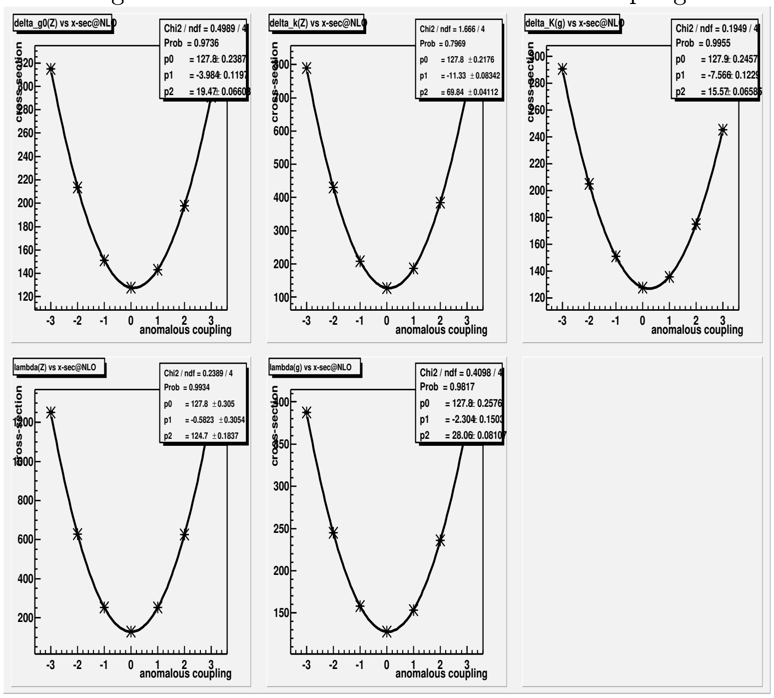

origin of this difference is still under investigation. [2]

4 WW Event selection and trigger

4.1 Introduction

This section outlines the first look at run 2 data and the work so far done on reproducing the run 1 analysis and efficiencies and identifying areas that need further investigation. Specific attention is given to the events where one decay is leptonic and one hadronic; this process has a higher branching ratio than the purely leptonic channel, but suffers from larger backgrounds, namely W+2jets and Z+2jets.

The first step is the identification of W bosons and hence a understanding of the lepton identification efficiencies, both trigger and offline, will be essential for the final analysis.

4.2 High Pt Lepton trigger

A data sample containing events with high Pt leptons is formed by three triggers. The central electron trigger, the express W and the express Z trigger.

As discussed, the level one trigger decision has to be made very quickly and must construct objects from simple quantities that are easy and quick to measure. For the case of the central electron trigger an event must contain at least one “L1 electron” object determined by loose cuts on its electromagnetic energy and track Pt .

At level 2 and level 3, where additional and more accurate information is available for use in the definition of the objects, harder cuts are applied to the EM energy and track Pt to reduce the event rate further. The efficiency of these cuts

[2] The sudden drop at 15GeV in the MCFM distribution is due to internal cuts used by Campbell and Ellis to separate W+0jets from W+1jet events

is still being investigated and updated as more and better data is collected. Until then we are relying on the offline selection criteria being sufficiently harder such that the relative trigger efficiency is high.

The high pt lepton sample is then formed from these three triggers by additionally requiring that each event passes: EM transverse energy $>$ 20 GeV, track Pt $>$ 10GeV, the ratio of the hadronic energy to the electromagnetic energy(HAD/EM) $<$0.1, Iso$<$ 0.1 where Iso is the isolation variable defined as the ratio of excess Et (not belonging to the electron cluster) in a cone of 0.4 to the electron cluster Et.

The express W and Z triggers differ only at Level 3, where the W trigger contains an additional cut on the missing transverse energy of 15GeV and the Z trigger contains a cut on a second photon-like object.

4.3 Offline reconstruction

4.3.1 Reconstructing electrons

The current offline selection contains harder cuts on the quantities above and additional cuts on the number of hits in the COT, cuts on the matching shower-max cluster quality and on track position parameters. The total efficiency of this selections is currently found to be $86.3 \pm 3.4(stat)\%$[3].

4.3.2 Reconstructing W's from electrons

leptonically decaying W's are reconstructed by requiring that the event has at least one good electron as defined above and missing transverse energy of more than 25GeV. This selection is estimated to be approximately 92% efficient[3] where the main backgrounds are QCD processes, $W \to \tau\nu$ and $Z \to ee$. Any event passing these cuts can then be used to calculate the transverse mass of the W from the equation below:

$M_T = 2\sqrt{Pt(e) \times Pt(\nu) \times Cos(\Delta\phi)}$

This transverse mass distribution is shown in Fig 3 for a small sample of run 2 data. The detector acceptance for $W \to e\nu$ has been estimated through a Monte Carlo study to be $24.42\% \pm 0.08\%(stat)$ with as yet no evaluation of the systematic uncertainties[3].

4.3.3 WW event selection

The run 1 WW selection has been applied to run 2 signal Monte Carlo and a sample of run 2 data. The run 1 selection of $WW \to e\nu e\nu$ gives an efficiency of 10% when applied to simulated run 2 signal data; no real events have yet been observed in run 2 data. The run 1 selection of $WW \to e\nu jj$ events proceeds by first requiring one leptonic decay and then searching for a hadronic W decay. Hadronically decaying W's are selected by taking the two highest Et jets and demanding that they each have a Pt greater than 30GeV and that their combined mass be in the window $60 < M_w < 110GeV$. To suppress the various backgrounds, such as W+2 jets, a pt cut on the transverse momentum of the hadronic W is applied. This cut is designed to utilise the higher cross-section of signal over background at high values of the boson pt distribution[5]. In run 1 this cut was placed such that only one background event was expected to pass. In the $67pb^{-1}$ of run 1a data, this cut was found to be optimal at 130GeV and in the combined $100pb^{-1}$ of run 1a and 1b data it was placed at 200GeV.

No events were found in the original run 1 analysis and the reproduction of this analysis on the sample of run 2 data also gave no events for a cut at 200GeV. The pt distribution of the run 2 events that pass all selections *except* the jet-jet pt cut is shown in Fig 4. Two events are seen at high pt(140GeV and 120GeV) but until a

Figure 3: Transverse Mass(GeV) of W candidates (number of events)

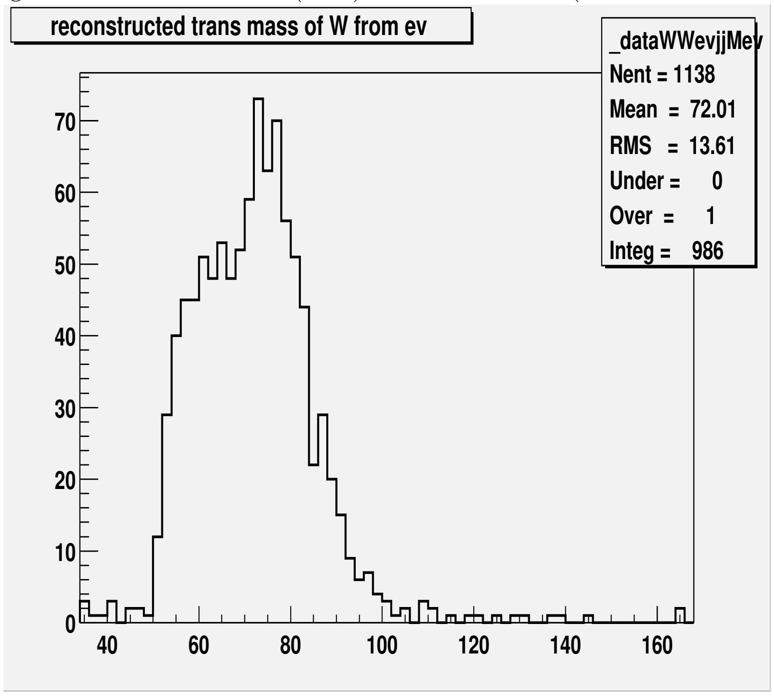

study of the background is done for run 2 it is not possible to conclude that these two events are $WW \to e\nu jj$ candidates.

5 conclusions and further work

A discussion of the run 2 upgrades has been presented along with an outline of the preliminary results of a measurement of the WW pair production cross-section at the Tevatron. The reproduction of the run 1 analysis on a sample of run 2 data yielded no events. further work in this direction will involve a study of the backgrounds to $WW \to e\nu jj$ in run 2 to allow the pt cut on the hadronically decaying W to be optimised. In the long term, advanced analysis techniques, such as neural networks, will be employed to try to improve the measurement of this decay channel.

A discussion of two next to leading order calculations of these WW processes was given, showing some discrepancies between the distributions predicted by these programs that is still under investigation. The next steps will involve a comparison of the two calculations with pythia and in the long term the conversion of MCFM into a full event generator.

References

[1] The ALEPH Callaboration. hep-ph/0104034.

[2] The CDF Callaboration. *Technical Design Report.* 1988.

[3] The CDF Callaboration. unpublished, 2002.

[4] Terrano Ellis, Ross. Nucl. Phys. B178 , 421, 1981.

[5] U Baur et al. Phys. Rev. D53 1098, 1996.

Figure 4: Transverse Momentum(GeV) of jet-jet pair in $WW \rightarrow e\nu jj$ data candidates

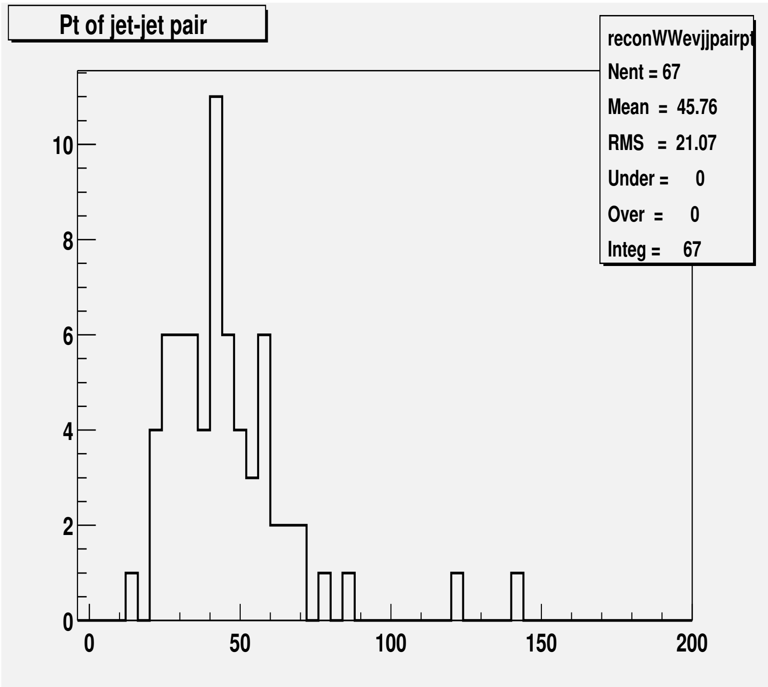

[6] S Frixione. Nucl. Phys. B140 280, 1993.

[7] R K Ellis J Capmbell. hep-ph/0006304 v1.

[8] J Woodside K Hagiwara and D Zeppenfield. Phys Rev D42 2113, 1990.

[9] Dixon Kunset and Signer. 1999.

[10] J Ohnemus. Phys. Rev. D44 1403, 1991.

Figure 5: Pt of $W^+$and W^- and WW pair (GeV Normalised to the cross-section) MCFM=red,BHO=black.

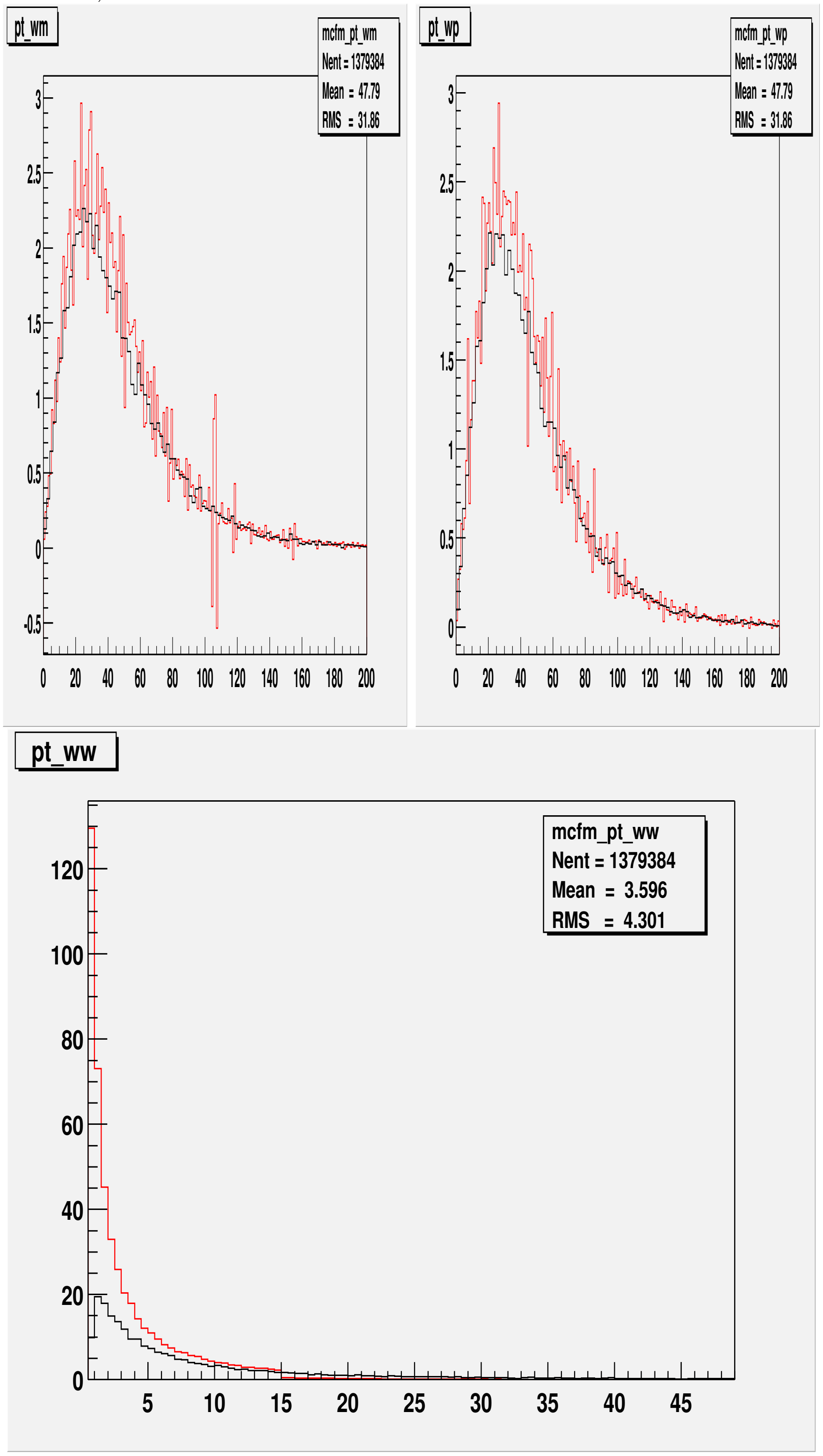

Figure 6: Mass of the WW pair in GeV Normalised to the cross-section. MCFM=red;BHO=black

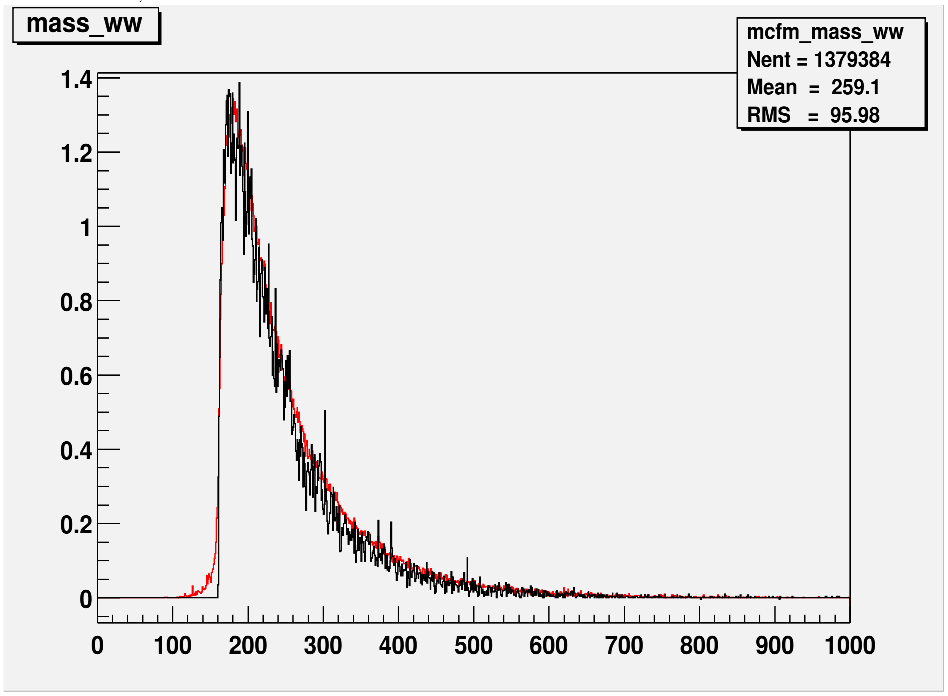

Figure 7: Rapidity distribution of the electrons and positrons normalised to the cross-section. MCFM=red; BHO=black

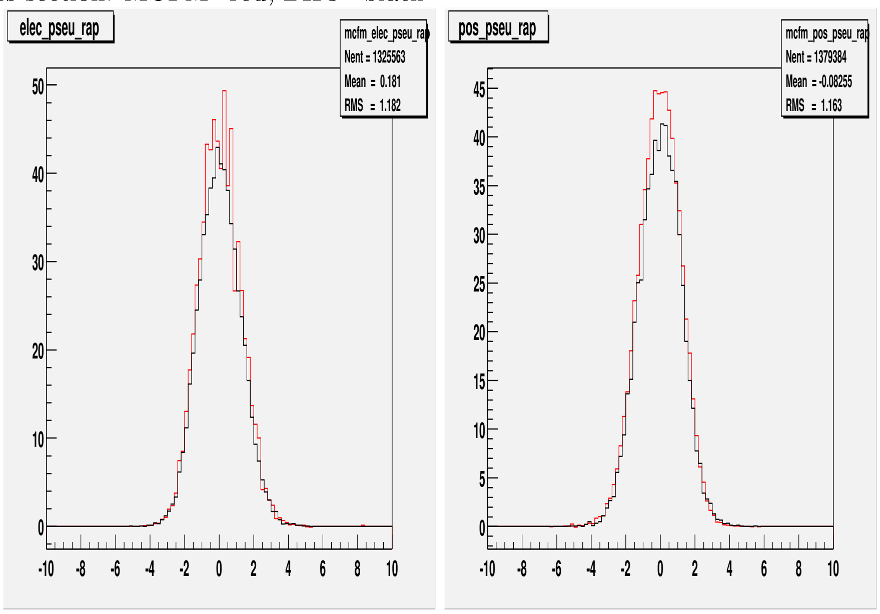

Fig 8 Diboson Production at the Tevatron